**Paper**

# Detent Force Calculations of a PMLSM using the Finite Element Method

Ghislain REMY*, Non-Member
Guillaume KREBS**, Non-Member
Abdelmounaïm TOUNZI**, Non-Member
Pierre-Jean BARRE*, Non-Member

This paper presents a Finite Element Analysis of a Permanent Magnet Linear Synchronous Motor. The aim is to obtain an accurate estimation of the detent force without oversize computation. First, some usual techniques dedicated to the calculation of the forces in electromagnetic devices, such as the Virtual Work Method and the Maxwell Stress Tensor, are described. Some keypoints of the meshing method using a commercial FEM software are presented and used in order to improve the thrust computations. After that, the topology and features of the studied motor are described to highlight specific problems of the modelling process. In the 2D FEM case, new meshing techniques are proposed, according to the force calculations. The FEM results obtained from the different methods are analysed and compared with the experimental ones. Second, using FEM results, a study of the independence of the cogging and the end-effect forces is presented. Particularly, an original approach is suggested in order to compute the cogging force only, using the same mesh for each motion step. Then, the PMLSM geometry is adapted to calculate the end-effect forces only.

**Keywords**: Finite Element Method, PMLSM, Meshing Techniques, Thrust computations, Cogging Force, End-effect Force, Detent Force

## 1. Introduction

Permanent Magnet Linear Synchronous Motors (ironcore PMLSM) are widely used in applications involving very high performances in terms of dynamics, high speed and accurate positioning[1]. Indeed, rare earth permanent magnets permit to reach high power to weight ratio. However, they suffer from cogging forces, due to the presence of slots in the primary. Furthermore, the extremities of the short primary induce end-effect forces. Both forces compose the detent force[2] and lead to vibrations and problems in achieving efficient control at low speeds without specific compensations[3][4].

The studies of the cogging force for electrical machines (rotary and linear)[5] are numerous compared to a small number of investigations on the study and the minimization of the end-effect forces of linear actutators[6]. Besides, their physical origin is not very well known and the solutions given to limit them are often issued from experimental tests.

Nowadays, Finite Element Method (FEM) is frequently encountered to study the behaviour of electromagnetic devices[7]. This numerical approach takes account of the real geometry and the non linearity of the magnetic material, which leads to accurate results with regard to the real system. Then, it can constitute a prevailing tool to study accurately the no-load forces and then to optimize PMLSM to reduce these forces.

Generally, in the case of global electrical characteristics, such as fluxes or electromotive forces, the quality of the mesh does not greatly affect the results. This is not the case of the no-load torque or force. Indeed, accurate calculations are highly dependent, on one hand, on the method used to perform them and, on the other hand, on the mesh quality and density of the modelled part of the device. Hence, one has to take care of these parameters to reach useful results, especially given that the no-load torque or force are generally very difficult to obtain from measurements. These difficulties are increased in the case of the permanent magnet linear synchronous machines, as the no load force is composed of two parts, the cogging and the extremity ones[8].

In this paper, we propose to use the FEM to study the cogging forces and the end-effect forces that compose the no-load detent forces.

In the first part, we introduce the formulations that are generally used to calculate the forces in the FEM codes. The problem of the force accuracy calculation induced by the meshing size is considered. An elementary part of the PMLSM is defined and modelled, and the main geometrical characteristics are explained. Thus, a meshing procedure of a PMLSM, intended to accurately calculate the no-load force using the FEM, is proposed.

The second part is devoted to the validation of the proposed procedure. The studied PMLSM is first presented. The results obtained from different meshes are analyzed. Some comparisons are carried out on the effectiveness of force formulations, the accuracy of the results and the time calculations. Then, the results obtained by the different simulations are compared to measurements carried out on the studied PMLSM.

Using the developped model, the no-load forces of the actuator are analysed. As a consequence, the ripple force due only to the reluctance variation of the air-gap is studied first. Then, identically, the force introduced by the extremities is analysed. Influent geometrical parameters of a particular PMLSM are considered. Hence, once the geometrical parameters inducing the end-effect force are well known, it will be easier to adapt them to reduce these no-load forces.

* Ecole Nationale Supérieure d'Arts et Métiers, Lille, France
** Université des Sciences et Techniques de Lille, France
Laboratoire d'Electrotechnique et d'Electronique de Puissance de Lille (L2EP) Tel: (33)320.622.246, fax: (33)320.622.759
e-mail: barre@lille.ensam.fr

## 2. The force calculation using the Finite Element Method (FEM)

To calculate the forces in electromagnetic systems, different methods can be used[9]. However, in most commercial FEM codes, only two approaches are generally used: the Virtual Work Method[10] and the Maxwell Stress Tensor[11].

**2.1 The Virtual Work Method** This approach is based on the transformation of magnetic energy into mechanical energy. We can show that the total force $F_s$ in one direction $s$ is obtained from the magnetic energy variation $W$ of the system after a displacement in this direction. The motion is performed at constant flux[12]~[14]. A similar expression can be deduced from the variations of the co-energy $W'$ at a constant current $i$, with the co-energy $W'$ calculated using an integration over a volume $v$ inside a domain $D'$ of the induction $b$ and the magnetic field $h$.

$$F_s = \frac{\partial W'}{\partial s} \Big| i = const., \quad \text{with} \quad W' = \int_{D'} \int_0^h b \, dh \, dv \quad \cdots\cdots\cdots\cdots (1)$$

Different techniques can then be used to compute such forces:

- A first method requires two solutions of the problem, one for each position. Then, from both energy values, the force can be deduced using Eq. 1. Even if a very fine mesh is not needed for this method, numerical errors can appear if the displacement step (for the calculation of the derivate) is too high[15].
- A second method is to carry out one computation of the problem only. Given the different fields on each element, then the magnetic energy is calculated for two positions of an object.
- Similarly, a third method consists in taking an air layer surrounding an object. The nodes of the layer are then virtually displaced. The energy is then calculated for each deformation[15].

Pratically, in commercial FEM softwares, the VWM formulation is performed using volume integration of a 3D mesh, or using surface integration of a 2D mesh. Therefore, it seems appropriate to have a regular mesh for the mobile part.

**2.2 The Maxwell Stress Tensor** In the case of the Maxwell Stress Tensor (MST), the following tensor is calculated:

$$T_{ij} = \mu_0 (H_i H_j - \frac{1}{2} \delta_{ij} H^2) \quad \text{with} \quad i, j = x, y, z \quad \cdots\cdots\cdots\cdots (2)$$

Where $H$ represents the magnetic field given by its components in the Cartesian frame (x,y,z) $H(H_x \; H_y \; H_z)$. $\delta_{ij}$ is the Kronecker sign ($\delta_{ij}$ =1 if $i$=$j$ otherwise $\delta_{ij}$ = 0).

For the Maxwell Stress Tensor approach, the force is calcultated using a surface integration on Γ', over a D' domain. The force can then be calculated using the divergence of the MST[16]:

$$F = \int_D \mathrm{div} \boldsymbol{T} \mathrm{d}v = \oint_{\Gamma'} \mu_0 ((\boldsymbol{H}.\boldsymbol{n})\boldsymbol{H} - \frac{1}{2}|\boldsymbol{H}|^2 \boldsymbol{n}) \mathrm{d}s \quad \cdots\cdots\cdots\cdots (3)$$

Where the vector $\boldsymbol{n}$ is the normal on the surface Γ'. The classical formulation detailed in Eq. 3 induces that the permeability has to be equal to the constant air permeability. So the force calculation has to be performed in an air region surrounding the studied part. The Maxwell Stress Tensor presents several advantages. Indeed, linear or non linear cases can be evaluated, and only the meshed part of the surface integration Γ' is concerned.

However, this method is very sensitive to the mesh quality and density of the region where the surface integration is taken. It is then preferable to have enough air layers on the D' domain surrounding the parts on which the forces have to be calculated. This is particularly the case in the air-gap areas, where high field changes usually occur. We notice that acceptable results can be obtained with at least 3 air layers.

**2.3 Other methods** Added to the VWM and the MST, other methods are used, less frequently, in FE codes to calculate the force. We can refer to the eggshell method[11], the equivalent magnetizing current for the force calculation[17] and the equivalent magnetic mass method[18]. Such methods are not yet frequently automatized in commercial FEM software. Furthermore, the mesh design has to be seriously considered, especially for the force calculations.

**2.4 Typical problems encountered using the force calculations** When calculating the forces, often some accuracy issues occur at the no-load operating point. The most common are the following:

- A calculation offset on the no-load force. This offset is generally the consequence of a meshing effect that is unrefined, not uniform and not homogeneous.
- The inaccuracy related to the force harmonics. This is typically due to an unrefined meshing coupled to a too much high displacement step.

To highlight these two problems, Fig. 1 presents the no-load force $T_{det}$ as a function of the displacement $x$. This detent force is calculated in the case of the studied structure with the MST formulation. These results are obtained using FEM analysis with a meshed part constituted of 26525 nodes and 52592 elements. Moreover, the calculation time for each position step is equal to 118s with a 3GHz and 1GB RAMBUS computer. The average value of this force of about 8N is only due to the bad quality of the mesh, whereas physically the value is null. On the other hand, to improve the study of the force ripple, a finer displacement step should be selected.

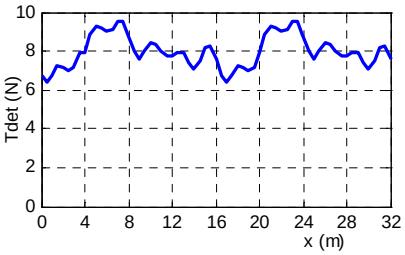


Fig. 1. Detent force with MST formulation

## 3. Meshing techniques for the force calculation

**3.1 Presentation of the studied PMLSM** The studied system is a LMD10-050 linear motor from the ETEL Company as shown in Fig. 2.

Fig. 2. LMD10-050 from ETEL company

The secondary is composed of a set of alternating Nd-Fe-B magnets, with a residual flux density $B_r$ of about 1.23T. Fig. 3 shows a cutting view of the whole studied PMLSM and Table 1 gives its main dimensions and specifications. The pole pitch $\tau_p$ is defined as the distance between two consecutives magnetic poles (N-S magnets).

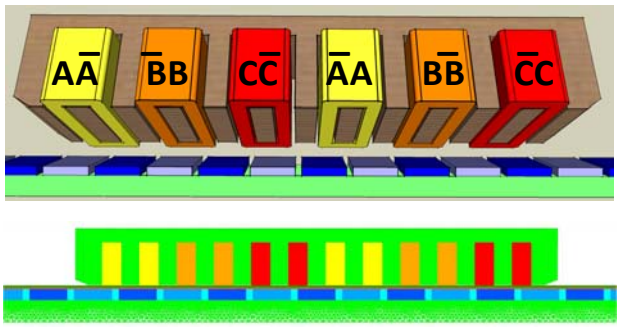


Fig. 3. 3D and 2D views of the studied PMLSM[19]

Table 1. Size and features of the analysed model

| Parameter | Value [Unit] |
|---|---|
| Number of poles | 2 |
| Residual flux density | 1.23 [T] |
| Height of PM | 4 [mm] |
| Length of PM | 50 [mm] |
| Width of PM | 14 [mm] |
| Pole pitch | 16 [mm] |
| Length of air-gap | 0.8 [mm] |

The no-load forces along the motion direction are generally very low when compared to attractive forces. In the case of the studied PMLSM, attractive forces are about 1770N while the no-load detent force is estimated at 4N[20].

**3.2 Geometry and mesh methodology** Here, we briefly propose a mesh procedure that could lead to an accurate force calculation: since there is a lot of direction fluctuation of the flux density in the air-gap, it is necessary to represent this active zone with at least three layers. So, the meshing size has to be chosen first in the air-gap, and then it can be larger everywhere else. Furthermore, for the force calculation, a fine cover of meshed air greatly improves the results. This approach is akin to the eggshell method[11] in improving the quality of the force calculation around the selected object. Fig. 4 shows a mesh designed for the LMD10-050 actuator.

The added numbers on Fig. 4 correspond to zones with different mesh sizes. The rule is to mesh only the zones which undergo fast density changes.

Fig. 5 shows a zoom of Fig. 4. We notice in Zone 4, called the air eggshell, that a 0.3mm mesh is particularly efficient (compared to 0.8mm in the air gap). This air eggshell acts as a cover on the primary ironcore, and permits us to follow the curve of the magnet induced flux more accurately. The other zones are defined with a larger mesh size of 0.8mm, with an auto-adaptation of the mesh to connect with the finer-meshed Zone 4 of the air eggshell.

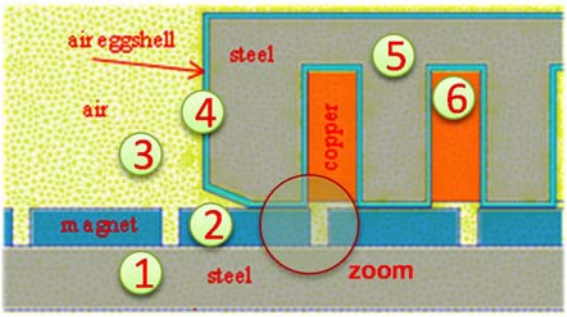


Fig. 4. Geometry with mesh size of 0.3 mm
1 – Iron; 2 – Nd-Fe-B Magnets; 3 – Air
4 – Air Eggshell; 5 – Iron Laminated sheet; 6 Copper

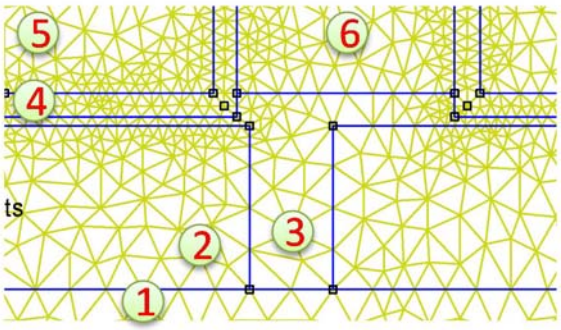


Fig. 5. Zoom of Fig. 4

About the force formulations for the Maxwell Stress Tensor, the calculation uses an integral of the volume of the primary laminated steel. For the Virtual Work Method, the variation of the co-energy is calculated over the whole system for more accurate results.

**3.3 Manual mesh optimization** Table 2 shows results of the detent force using the MST and the VWM for different mesh sizes of the geometry, using a re-meshing process.

The meshing size has a direct influence on the value of the detent force. To obtain the force offset value, two approaches can be used. In the first one, calculations are performed at a position of the moving part, where the detent force is nil from a physical point of view. In the case of the studied PMLSM, it would be the position shown in Fig. 2. The second one consists first in calculating the detent force under displacement, then in determining the average value on a periodic part of the detent force waveform. Using the MST and the VWM, we have calculated the detent force offset for different cases.

We notice in Table 2 that a smaller mesh size is not always the best solution. Therefore, the system mesh is a predominant factor, as it directly influences the numerical errors.

**3.4 Detent force results** Besides the quality of the mesh, the calculation of the detent forces is also very sensitive to the displacement method. Different techniques can be used to simulate the movement in FEM . The results are generally more accurate, with no change in mesh between two steps. In magnetostatic cases, the motion can also be performed by permuting some materials (the magnets in our study).

Moreover, the non linearity of the magnetic material can have effects on the result accuracy. Fig. 6 shows the nonlinear magnetic curve *B-H* of the ferromagnetic sheets[21].

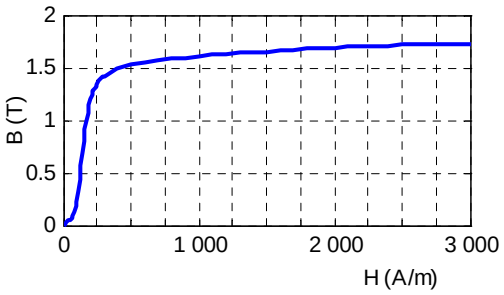


Fig. 6. *B-H* curve of the laminated sheet

Studies at no load have been performed using a free FEM package. Fig. 7 shows the magnetic flux density in the cutting plane given in Fig. 4. We can clearly notice the concentration of the flux density in the teeth of the primary, as well as the leakage flux inside the slots. This constitutes one of the origins of the detent force.

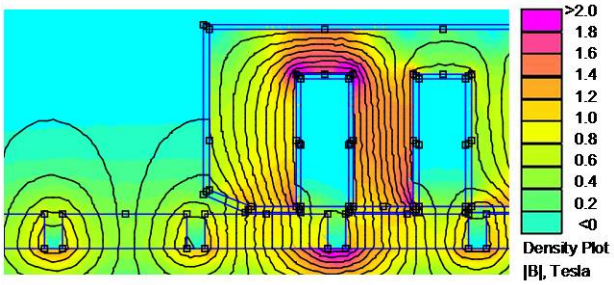


Fig. 7. Flux induction field

Fig. 8 shows the no-load force calculated using the MST for a linear and a non-linear case. We notice, in this particular case, that the results are very close. So, to minimise computation time, only the linear case is then studied.

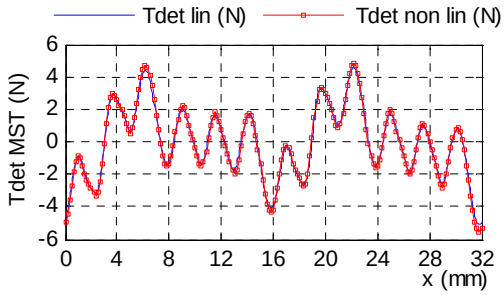


Fig. 8. No load force of a LMD10-050 (ETEL)

Fig. 9 presents the results of the no-load force calculated by both approaches (VWM and MST) in the linear case: we can notice on the waveform that both methods are in good agreement.

Then, a Fast-Fourier Transform (FFT) is applied on both the Fig. 9 results. The harmonic values Hn of the detent force are presented in Table 3. We notice that the results on harmonics H1 and H12 are close to 8% apart between both formulations.

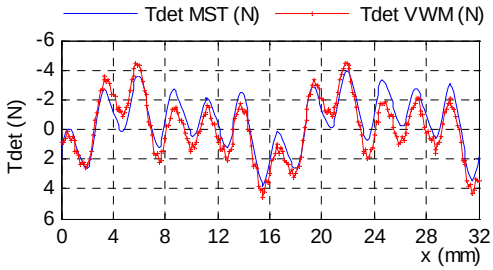


Fig. 9. Detent force calculations with both methods

Table 3. Comparison of harmonics for both formulations

| Formulation | H1 | H2 | H3 | H4 | H12 | H24 |
|---|---|---|---|---|---|---|
| Maxwell (N) Stress Tensor | 1.36 | 0.90 | 0.35 | 0.39 | 1.84 | 0.21 |
| Virtual Work Method (N) | 1.48 | 1.44 | 0.40 | 0.43 | 1.78 | 0.17 |

We notice several harmonics on the Fast-Fourier Transform (FFT) results presented in Table 3. More explanations of the origin of the detent force and the optimization of the PMLSM design can be found in the literature[21].

**3.5 Experimental validation** The proposed model is experimentally verified on a laboratory test system equipped with an ETEL LMD10-050 linear motor (Fig. 1). We have used a Heidenhain exposed linear encoder with a grating period of 20µm to detect the mover position. We have also used a dSPACE DS1005 real-time card for the identification procedures. The linear motor is star-connected, with an accessible neutral wire. The specifications of the test system are given in Table 4:

Table 4. Specifications of the Test Bench[20]

| Rated Current | Maximal Current | Force Constant Kt |
|---|---|---|
| 2 Arms | 7.9 Arms | 88.8 N/Arms |
| **Rated Thrust** | **Maximal Thrust** | **Attraction Force** |
| 130 N | 554 N | 1770 N |

The detent force is estimated using Newton's 2nd law:

$$M\frac{dv}{dt} = T_{em} - T_{\det} - T_{Coul} - T_{vis} - T_{load} \quad \cdots\cdots (4)$$

With $T_{det}$, the detent force, $T_{load}$, the load force, $T_{Coul}$, the Coulomb force, $T_{vis} = f_{vis} * v$, the viscous friction force, with $f_{vis}$, the viscous coefficient; $M$, the mobile mass, $v$, the primary velocity and $T_{em}$, the electromagnetic thrust.

Table 5 shows the numerical values of the parameters and the estimated accuracy obtained from experimental identification.

Table 5. Values of the estimated parameters

| Parameter | Value | Accuracy |
|---|---|---|
| $T_{Coul}$ | 15N | 1N |
| $f_{vis}$ | 15N/(m/s) | 0.5N/(m/s) |
| $M$ | 3.6kg | 0.2kg |

In order to simplify the detent force identification, tests are performed at no-load, $T_{load} = 0$.

Due to the non-linear friction phenomena at low-speed, a minimum speed of 0.1m/s is necessary to validate the assumptions that $T_{Coul}$ and $f_{vis}$ are constant.

Furthermore, identifications at constant speed reduce the influence of the inaccuracy of the estimated mobile mass and of the estimated viscous friction coefficient.

The thrust estimation $T_{em}$ is obtained by the equation[22]:

$$T_{em} = \frac{d\phi_{Ma}(x)}{dx} \cdot i_a + \frac{d\phi_{Mb}(x)}{dx} \cdot i_b + \frac{d\phi_{Mc}(x)}{dx} \cdot i_c \quad \cdots\cdots\cdots (5)$$

Where $\phi_{Ma}$, $\phi_{Mb}$, $\phi_{Mc}$ are the fluxes induced by a magnet in the phase *a, b* and *c* respectively; $i_a$, $i_b$, $i_c$ are the three phase currents.

The magnet flux has been identified with only 3% of the fundamental for the 5th harmonic[23], so the back-electromotive force waveform can be simplified into a sinusoid:

$$\frac{d\phi_{Ma}(x)}{dx} = \hat{\phi}_M \cdot \frac{\pi}{\tau_p} \cdot \sin\left(\frac{\pi}{\tau_p} \cdot x\right) \quad \cdots\cdots\cdots\cdots\cdots\cdots\cdots (6)$$

Where $\hat{\phi}_M$ is the maximum flux induced by a magnet in phase *a*.

An important difficulty in estimating the detent force is to eliminate offsets and noises on current measurements. Indeed, in the studied system, the minimum offset level and the noise level are both about 20mA. Using Eq.5 and Eq.6 and with a maximum flux of about 0.23Wb[23], an offset of about 0.9N appears on the estimated thrust. So, an accurate identification of the detent force is only available by using filtering techniques and offset compensation on the current measurements.

Fig. 10 shows the no-load force waveform measured on the actuator. Some fast force peaks are still visible in Fig. 10, due to the Power Electronic commutations. However, we notice the good agreement between the simulation results and the measurements.

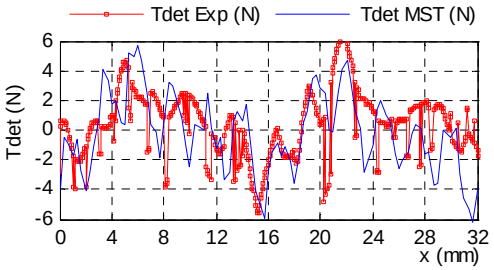


Fig. 10. Experimental estimation of the detent force

Thus, the model can be used in order to analyse both forces more accurately and to minimise these no-load forces by optimising the device geometry.

**3.6 Conclusion on the force calculation** To obtain accurate detent force calculations, meshing techniques, force formulations and movement techniques have to be carefully chosen.

As the VWM formulation is performed using integration over all of the primary iron core rather than its periphery, it is less sensitive to the imperfect field path caused by the underestimation of the meshing size. Nevertheless, force results are not good enough to neglect offsets.

## 4. Analysis of the detent force

The goal of this part is to highlight the geometrical parameters involved in the cogging and the end-effect forces. Then, it is necessary to study them separately. To do this, we have subdivided the PMLSM into two modelled parts, which allows us to calculate both components of the detent force independently. With the FEMM software[15], there are no specific techniques for the force calculations under movement. But two different techniques can be applied to calculate the force under displacement using the FEM. The main differences are the application of the boundary conditions dedicated to the movement:

- Half periodic conditions on the air-gap side with a locked-step approach[24],
- Two sets of periodic conditions with circular permutation of the periodicity conditions[25].

The first method requires a re-meshing at each step and an offset value can occur on the force results[26].

The second technique is presented in the following part for the calculation of the cogging force.

The locked-step approach consists in permutating the calculation unknowns associated to a common line (in the 2D case) or to a common surface (in the 3D case) between the static and the mobile part. Therfore, it requires a regular mesh (i.e. with a regular step). Unfortunately, this method induces a very constrained mesh in the 3D case. Its main advantage is to eliminate, in the force calculation, the force error induced by the re-meshing process.

**4.1 Device for the cogging force calculation** Experience shows that it is better to have the same mesh during each step motion[27]. Indeed, this reduces the computation errors for meshes with a small number of elements and maintains the errors on the force calculations constant. So, the force results using the FEM can be set free by this offset.

In order to avoid meshing the system at each step, we present an appropriate technique. Fig. 11 shows the central part of the linear actuator geometry.

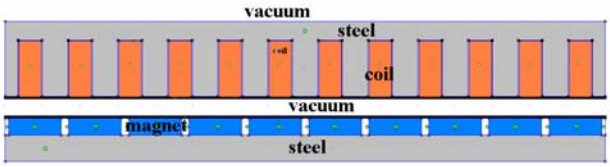


Fig. 11. Geometry for cogging force calculation[28]

Two sets of periodic conditions are applied. The first ones, on the lateral sides, allow us to suppose that the device is infinite. Hence, only the cogging forces are calculated. The other periodic conditions are dedicated to the movement. Fig. 12 shows a zoom where they are located on the upper and lower sides of the air-gap. Then, the movement is simulated by a circular permutation of the n periodic conditions located in the lower side of the air-gap:

$$\begin{aligned} &\textit{upper side}: \quad c_1, c_2, \ldots, c_{n-1}, c_n \rightarrow c_1, c_2, \ldots, c_{n-1}, c_n \\ &\textit{lower side}: \quad c_1, c_2, \ldots, c_{n-1}, c_n \rightarrow c_n, c_1, \ldots, c_{n-2}, c_{n-1} \end{aligned} \quad \cdots (7)$$

This method is equivalent to the locked-step approach. Indeed, as only the periodic conditions change between two calculation steps, the mesh process occurs only once, and errors induced by the remeshing process on the force calculations are avoided.

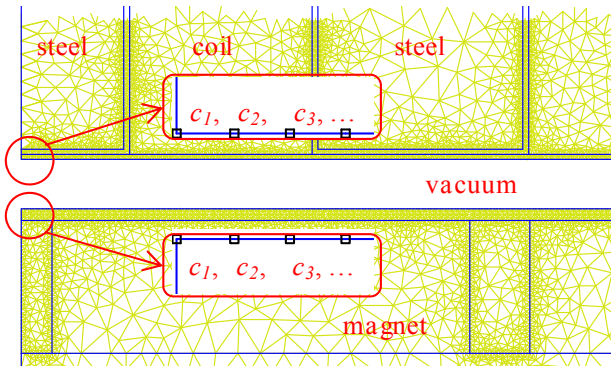


Fig. 12. Permutation of the n periodic conditions

**4.2 Device for the end-effect forces calculation** Some studies for the primary shape have been done on the design of edge shape to reduce the detent force:

- Optimization of the mover length[29].
- Smooth formed edge shape[19].
- Skewing only the ends of the armature[29].

But, as the analytical approach is complex, a mathematical expression of the edge shape has not yet been worked out.

To analyse the end-effect forces, the whole primary is modelled and the slots are replaced by iron. In fact, the entire primary is considered as one steel block. Fig. 13 shows that the extremities are inclined with an angle $\vartheta_{ext}$ of about 20°.

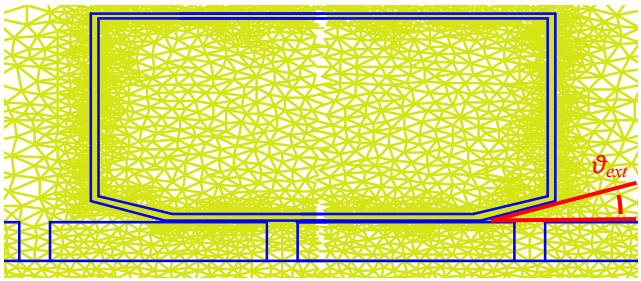


Fig. 13. Straight shape of the primary extremities[26]

**4.3 Force analyses**

Using the same free 2D-FEM software, calculations have been performed to obtain the forces on both modeled parts. The results are given below in the case of a linear magnetic material curve. Fig. 14 shows the cogging force calculated using the Maxwell Stress Tensor formulation obtained with the mesh from Fig. 11:

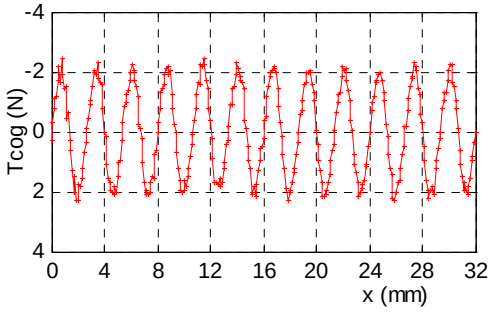


Fig. 14. Cogging force using the geometry of Fig. 11

We notice that this force has a sinusoidal waveform with a period $\tau_{cog}$ of 2.33mm. This corresponds to the greatest common divisor "gcd" of the tooth pitch ($\tau_{tooth}$ = 80/6 mm) and the pole pitch ($\tau_p$ = 16mm). According to the design presented in Fig. 11, the period of the cogging force will be:

$$\tau_{cog} = \tau_p \cdot \tau_{tooth} / \tau_{common} \quad \cdots\cdots (8)$$

Where $\tau_{common}$= 80mm is the first common period between pole pitch and tooth pitch. Hence, the cogging force period is $\tau_{cog}$ = 8/3mm as in Fig. 14.

Fig. 15 gives the waveform of the end-effect force, calculated using the same formulation, with the modelled part given in Fig. 13.

Here, the end-effect force is a sum between two saw-tooth forces due to the magnets and the extremities of the steel block. We can clearly see the periodicity of this force, which is 16mm.

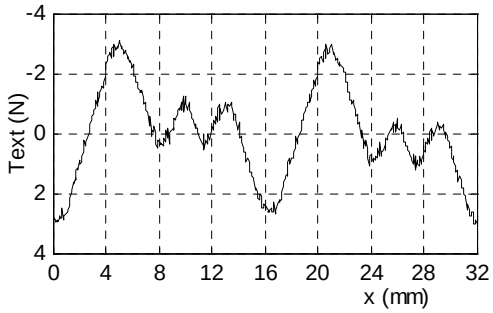


Fig. 15. End effect force using the geometry of Fig. 13

As the regions where the cogging and the end-effect forces act are clearly separated, and as we have used a linear *B-H* curve for the ferromagnetic material, the sum of both cogging and end-effect forces gives us the total no-load force. Fig. 16 presents this sum compared to the no-load force obtained directly when the whole device is modeled. We can see that the results are close enough to validate the suggested method. Even if an influence of the slot replacement for the end-effect force calculation occurs, the force results show that the sum of cogging and end-effect forces is close to the detent force. So, this influence seems to be negligible.

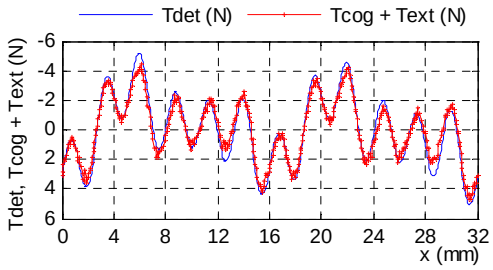


Fig. 16. Comparison between the sum of both forces and the total no-load force. (Linear case)

In order to analyse these forces, a Fast-Fourier Transform (FFT) has been performed on the detent force of Fig. 16. The results given in Fig. 17 show that the harmonics of the cogging force are dissociated from the ones of the end-effect force.

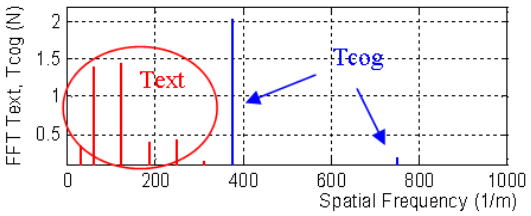


Fig. 17. FFT of the Detent force using the FEM

### 4.4 Discussion on the detent force reduction

In this part, only the influence of the geometry on the forces will be discussed. From a physical point of view, the main parameters involved in the cogging force and in the end-effect force can easily be identified.

Hence, the magnitude of the cogging force is influenced by:

- The ratio of magnet width to rotor pole pitch;
- The ratio of the tooth width to the stator pole width;

Skewing magnets is not possible in the case of the studied PMLSM. Indeed, it is a structure with an open slot mover and with different pole pair numbers on the primary and secondary. Most of the interaction between the magnetic fields is based on the reluctance of the airgap. In that case, skewing the teeth or the magnets would only lead to a reduction of this interaction and consequently of the PMLSM performances. However, it can be used for a classical PMLSM, which generally yields to a decrease of the cogging force magnitude, but this increases the complexity of the motor construction[28].

On the other hand, the magnitude of the end-effect force is caused by:

- Length of the primary;
- Shape of the extremity teeth

In the case of the studied PMLSM, we have performed some simulations with different shapes for the extremities. As presented in Fig. 13, the angle $\vartheta_{ext}$ can be optimized. Fig. 18 shows on the obtained results that an angle $\vartheta_{ext}$ of 20° leads to a significant decrease of the detent force.

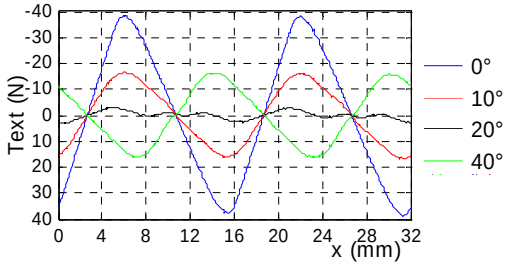


Fig. 18. $T_{ext}$ using FEM with different angles of the extremities tooth

## 5. Conclusion

In this paper, we have used a 2D finite-element software package to analyse the cogging and the end-effect forces of a permanent magnet linear synchronous motor.

First, we have presented some calculation techniques used in the FEM to calculate the forces. Then, we have underlined the problems which are generally encountered in force calculations. The main one is the mesh quality. A mesh technique has been introduced in order to reach accurate results for the no load force.

It appears that at least three layers in the airgap seem appropriate to reduce the computation error on the force offset.

This technique has then been used to study the behaviour of a PMLSM. Both the VWM and MST formulations give good results. FEM results show that the MST formulation is slightly more accurate, but is also more sensitive to the mesh quality than the VWM formulation, which is calculated with the whole system. After detailing the experimental procedures to estimate the no-load force, we have validated the model using the experimental results.

Then, to analyse each force separately, we have subdivided the PMLSM into two modelled parts. We have shown that the sum of both forces gives the total no-load force. Therefore, using each of the modelled parts, it is possible to optimise the geometrical parameters in order to reduce the cogging and end-effect forces separately. In the last part, we have presented the most influent geometric parameters on the no-load force. Future work will focus on the optimization of the tooth extremities to reduce the detent force, while keeping the inductances symmetrical for a 3-phase PMLSM.

## Acknowledgement

This work has been supported by Ralph Coleman of ETEL's Motion Control Research Team, who works actively with the L2EP (Laboratory of Electrical Engineering and Power electronics) of Lille, France.

(Manuscript received Oct. 18, 2007, revised Oct. 18, 2007)

## References

(1) J.F. Gieras and Z.J. Piech, "Linear Synchronous Motors, Transportation and Automation Systems", CRC Press (Sept. 1999)

(2) T. Yoshimura, H. J.Kim, M. Watada, S. Torii, and D. Ebihara, "Analysis of the reduction of detent force in a permanent magnet linear synchronous motor", IEEE Trans. Magn., Vol.31, pp. 3737-3739 (1995)

(3) Y.W. Zhu and Y.H Cho, "Thrust Ripples Suppression of Permanent Magnet Linear Synchronous Motor", IEEE Trans. Magn., Vol.43, No.6 (June 2007)

(4) G. Martinez, J. Atencia, M. Martinez-Iturralde, A. Garcia Rico, and J. Florez, "Reduction of detent force in flat permanent magnet linear synchronous machines by means of three different methods", IEMDC'03, Vol.2, pp. 1105-1110 (June 2003)

(5) J.F. Gieras and M. Wing, "Permanent magnet motor technology – Design and Applications", Marcel Dekker, 2nd Ed ( 2002)

(6) M. Inoue and K. Sato, "An approach to a suitable stator length for minimizing the detent force of permanent magnet linear synchronous motors", IEEE Trans. Magn., Vol.36, No.4, Part 1 (Jul. 2000)

(7) A. Cassat, N. Corsi, N. Wavre, and R. Moser, "Direct Linear Drives: Market and Performance Status", LDIA2003, Birmingham, UK (8-10 Sept. 2003)

(8) I. Boldea and S. A. Nasar, "Linear Motion Electromagnetic Systems", Wiley, New-York (1985)

(9) A. Bossavit, "Force-related Nuts and Bolts in the Discretization Toolkit for Electromagnetics", COMPUMAG 2007, Aachen, Germany, pp.885-886 (June 2007)

(10) W.N. Fu, P. Zhou, D. Lin, S. Stanton, and Z.J. Cendes, "Magnetic Force Computation in Permanent Magnets Using a Local Energy Coordinate Derivative Method", IEEE Trans. Magn., Vol.40, No.2 (Mar. 2004)

(11) F. Henrotte, G. Deliège, and K. Hameyer, "The eggshell method for the computation of electromagnetic forces on rigid bodies in 2D and 3D", CEFC 2002, Italy (2002)

(12) J.L. Coulomb, "Methodology for the determination of global electromagnetic quantities from a finite element analysis and its application to the evaluation of magnetic forces, torques, and stiffness", IEEE Trans. Magn., Vol.19, No.6 (1983)

(13) J.L. Coulomb and G. Meunier, "Finite element implementation of virtual work principle for magnetic or electric force and torque computation", IEEE Trans. Magn., Vol.20, No.5 (1984)

(14) Z. Ren and A. Razek, "Local force computation in deformable bodies using edge elements", IEEE Trans. Magn., Vol.20, No.2 (1992)
(15) FEMM, user manual, http://femm.foster-miller.net (2008)
(16) A.N. Wignall, A.J. Gilbert, and S.J. Yang, "Calculation of forces on magnetised ferrous cores using the maxwell stress method", IEEE Trans. Magn., Vol.24, No.1 (Jan. 1988)
(17) G. Hennerger, P.K. Sattler, and D. Shen, "Nature of the equivalent magnetizing current for the force calculation", IEEE Trans Mag, Vol. 28, No.2 (1992)
(18) I.S. Jung, J. Hur, and D.S. Hyun, "3-D analysis of permanent magnet linear synchronous motor with magnet arrangement using equivalent magnetic circuit network method", IEEE Trans Mag, Vol.35 (1999)
(19) N. Wavre, "Permanent-Magnet Synchronous Motor", ETEL patent US 05642013A (Jun. 1997)
(20) LMD10-050 Datasheet, Etel, http://www.etel.ch (2007)
(21) G. Remy, G. Krebs, A. Tounzi, and P.J. Barre, "Finite Element Analysis of a PMLSM, Part 2: Cogging force and end-effect force calculations", LDIA2007, Lille, France (Sept. 2007)
(22) A.E. Fitzgerald, C. Kingsley, and S. Umans, "Electric Machinery", McGraw-Hill, 6th Ed. (Jul. 2002)
(23) G. Remy, A. Tounzi, P.J. Barre, F. Piriou, and J.P. Hautier, "Application of Finite-Element Method to a PMLSM with Non-Sinusoidal Electromotive Force", IEEJ Trans. IA, Vol.126, No.10 (Oct. 2006)
(24) I. S. Jung and S. B. Yoon et al., "Analysis of force in a short primary type and a short secondary type permanent magnet linear synchronous motor", in Conf. IEMDC '97, pp. MC1-8.1-MC1-8.3 (1997)
(25) G. Krebs, A. Tounzi, B. Pauwels, D. Willemot, and F. Piriou, "Two cogging force minimization applied to a linear actuator", ICEM2006, Chania, Greece (2006)
(26) G. Remy, G. Krebs. A. Tounzi, and P.J. Barre, "Finite Element Analysis of a PMLSM, Part 1: Meshing techniques and thrust computations", LDIA2007, Lille, France (Sept. 2007)
(27) S. Xiaodong Y. Le Menach, J.P. Ducreux, F. Piriou, "Comparison of slip surface and moving techniques for modelling movement in 3D with FEM", COMPEL, Vol.25, No.1, pp. 17-30 (Jan. 2006)
(28) N. Wavre, "Permanent Magnet Synchronous Motor", ETEL patent EP 0793870B2 (Jul. 1998)
(29) P.Q Yu, S. Liu, J.Z. Fu, and Z.C. Chen, "Analysis and reduction of detent force in permanent magnet linear synchronous motor", ICCEA2004,pp.525 (Nov. 2004)

**Ghislain REMY**  (Non-member) was born in Epinal, France on November 12, 1977. He received the teacher degree "agrégation" in 2001. He received a Ph. D degree in electrical engineering from ENSAM in 2007, and is presently an assistant professor at the Electrical Engineering Laboratory of Paris (LGEP), France. His current research interests include multiphysics modelling and control of actuators.

**Guillaume Krebs**  (Non-member) was born in Croix, France on May 27, 1978. He received the Engineer degree in 2003 and the Ph. D degree in electrical engineering from the University of Science and Technologies of Lille (USTL) in 2007. Presently, he works as assistant professor at the Electrical Engineering Laboratory of Paris (LGEP), France. His research areas are the design and the modelling of electrical machines and non destructive testing.

**Abdelmounaïm Tounzi**  (Non-member) was born in Casablanca (Morocco) in 1965. He graduated from the University of Nancy, France (M's 1989) and the 'Institut National Polytechnique de Lorraine' (INPL), France (PhD 1993). He has been a Professor at the University of Science and Technologies of Lille (USTL) since September 1993. His research areas are the design and modelling of electrical machines.

**Pierre-Jean Barre**  (Non-member) was born in France in 1957. He received the teacher degree "agrégation" in mechanical engineering in 1991 and the PhD in automatics in 1995 at the Ecole Nationale Supérieure d'Arts et Métier de Lille (ENSAM). He is currently Director and a Professor at the ENSAM of Lille His current research interests include automatics, robotics and motion control.

Table 2. Offset value on the detent forces using MST and VWM of Fig. 4

| Mesh size of zone number (mm) | | | | | | Offset Force (N) | | Number of | Number of |
|---|---|---|---|---|---|---|---|---|---|
| 1 | 2 | 3 | 4 | 5 | 6 | MST | VWM | Nodes | Elements |
| 1 | 1 | 1 | 0.25 | 1 | 1 | 7.87 | 1.32 | 26525 | 52592 |
| 0.8 | 0.8 | 0.8 | 0.5 | 0.8 | 0.8 | 6.66 | 1.319 | 38169 | 75878 |
| 0.8 | 0.8 | 7 | 0.3 | 0.8 | 0.8 | 0.04 | 1.33 | 33190 | 66033 |
| 0.8 | 1 | 7 | 0.3 | 0.8 | 0.8 | 0.023 | 1.34 | 30377 | 60411 |
| 0.8 | 1 | 7 | 0.3 | 0.8 | 1 | 0.058 | 1.281 | 30537 | 60731 |
| 0.8 | 1 | 7 | 0.3 | 2 | 1 | 0.058 | 1.282 | 30022 | 59701 |
| 2 | 1 | 7 | 0.3 | 2 | 1 | 0.086 | 1.254 | 27459 | 54632 |
| 0.8 | 0.8 | 0.8 | 0.3 | 0.8 | 0.8 | 0.067 | 0.694 | 44947 | 89434 |
| 0.8 | 0.8 | 0.8 | 0.25 | 0.8 | 0.8 | -1.65 | 3.079 | 54977 | 109494 |
| 0.8 | 0.8 | 0.8 | 0.15 | 0.8 | 0.8 | -1.77 | 0.883 | 84556 | 168652 |
| 0.8 | 0.8 | 0.6 | 0.15 | 0.8 | 0.8 | -1.723 | 0.808 | 95783 | 191067 |
| 0.8 | 0.8 | 0.3 | 0.15 | 0.8 | 0.8 | -1.828 | 0.952 | 174439 | 348242 |
| 0.8 | 0.8 | 0.8 | 0.1 | 0.8 | 0.8 | 0.0086 | 0.029 | 132336 | 264212 |